Journal of Inorganic Biochemistry 201 (2019) 110816

Contents lists available at ScienceDirect

Journal of Inorganic Biochemistry

journal homepage: www.elsevier.com/locate/jinorgbio

Synthesis and anticancer evaluation of benzo-N-heterocycles transition metal complexes against esophageal cancer cell lines

Shuangcheng Zhi[a], Yuyang Li[a], Jiaxu Qiang[a], Jiyong Hu[b], Wei Song[a], Jin'an Zhao[b,*]

[a] School of Life Science and Engineering, Henan University of Urban Construction, Pingdingshan 467036, Henan, PR China
[b] School of Material and Chemical Engineering, Henan University of Urban Construction, Pingdingshan 467036, Henan, PR China

ARTICLE INFO

Keywords:
Benzo-N-heterocycles
Transition metal complex
Cytotoxicity
Apoptosis

ABSTRACT

Three novel transition metal complexes, Cu(p-2-bmq)Cl_2 (**1**), Zn(p-2-bmq)Cl_2 (**2**) and [Co(p-2-bmq)Cl_2]$_2$ (**3**) (where p-2-bmq = 2-((1-(pyridin-2-yl)-1H-benzoimidazol-2-yl)methyl) quinolone, have been synthesized. The complexes were detected for their cytotoxicity *in vitro* against four human esophageal cancer cell lines (SMMC7721, BGC823, HCT116 and HT29) by MTT assay. The results showed that they all have anti-tumor cell proliferation activity. E specially, complex **1** exhibited significant cytotoxicity with IC_{50} value of 15.89 μM against SMMC7721 cells for 72 h. The morphological changes of nuclei by fluorescence staining methods proved that complex **1** could induce intracellular DNA damage. The flow cytometry analysis revealed that the treatment of SMMC7721 cells with complex **1** induced intracellular ROS increased, mitochondrial potential collapse, G2/M-phase arrest, and even apoptosis. These studies should highly valuable for the development of transition metal-based compounds to the potential anticancer medicinal applications.

1. Introduction

The potential of metal-based anticancer agents have been received widespread attention and exploration since the landmark application of cisplatin and related compounds in the clinic [1,2]. However, platinum-based chemotherapy drugs are accompanied by severe dose limitations and side effects, including neuro-, hepato- and nephrotoxicity [3]. Efforts are focused to develop novel metal-based compounds and explore its mechanism of action to alleviate these limitations [4,5]. The well-established biological properties of metal-based complexes are often characterized by a wide variety of coordination binding sites, ligand types, and central metal ion redox potential, which are easily to external form electrostatic or coordinate, groove or intercalative binding, with biological receptors [6–8]. Moreover, metal center complex can also subject for the design and synthesis of therapeutic or diagnostic drugs [9–11]. Since then, the potential of different metal-based chemotherapeutic drugs has been widely explored and especially transition metal complexes due to their oxidative nature and biocompatible properties [12–14].

There is also an extensive range of ligands that can be used to involve in biological activity, including target recognition, receptor binding domain, release of active monomer, and activation of effector points [15–17]. Benzimidazole derivatives have various biological activity and clinical applications, including antibacterial, antitumor, antiviral, antifungal, antihelmintic, antihistaminic, anticorrosin, and antihypertensive, *etc.* which are already used as crucial pharmacophore in drug discovery [18–21]. Recently, studying on the functional diversity of transition metal center combined with benzo-N-heterocycles derivatives has provided an inspiration for the development of novel chemotherapeutic agents. Mao group recently reported two new Cu(II)-dipeptide compounds of 2-(4′-thiazolyl)benzimidazole, [Cu(Gly-Gly)(TBZ)(Cl)]·4H_2O and [Cu(Gly-l-Leu)(TBZ)(Cl)]·H_2O (Gly-Gly = glycyl-glycine anion, Gly-l-Leu = glycyl-l-leucine anion, and TBZ = 2-(4′-thiazolyl)benzimidazole) have been prepared and evaluated, which were well intracellular DNA damage, ROS production, and even significantly cytotoxicity *in vitro* against HeLa cell line [22]. Moreover, two zinc(II) compounds of Zn(bpbp)Cl_2 and [Zn(bpbp)$_2$]$(ClO_4)_2$·CH_3CH_2OH·H_2O (bpbp = 2,6-bis(1-phenyl-1H-benzo[*d*]imidazol-2-yl)pyridine) with bis-benzimidazole-based ligands were prepared and evaluated for their *in vitro* antitumor activities. The complexes were showed significant antiproliferative against five human tumor cell lines by comparing with cisplatin [23]. Platinum-based antitumor drugs may still be essential used in clinic, however innovative approaches, altering various transition metals, are producing novel compounds to chemotherapy.

Actually, it is likely that the novel high efficiency, low system toxicity, high selectivity, and high antiproliferative transition metal compounds will retain a high level of research interest. The

* Corresponding author.
E-mail address: zjinan@zzu.edu.cn (J. Zhao).

https://doi.org/10.1016/j.jinorgbio.2019.110816
Received 18 February 2019; Received in revised form 28 August 2019; Accepted 1 September 2019
Available online 06 September 2019
0162-0134/

mechanisms of benzo-N-heterocycles-based transition metal compounds with antitumor activity still need further exploration, and this field with pyridine-benzimidazole-quinoline ligand has rarely reported. Hence, three novel compounds Cu(p-2-bmq)Cl_2 (**1**), Zn(p-2-bmq)Cl_2 (**2**) and [Co(p-2-bmq)Cl_2]$_2$ (**3**) with pyridine-benzimidazole-quinolinyl ligand have been synthesized and *in vitro* biological activities have been investigated. Elucidation of the detailed antitumor mechanisms will accelerate metal-based chemotherapeutic agents discovery and lead to further developments of this field.

2. Experimental section

2.1. Materials and measurements

All reagents and chemicals were used as received without further purification. 3-(4,5-dimathylthiazol-2-yl)-2,5-diphenyltetrazolium bromide (MTT), ethidiumbromide (EtBr), and Calf thymus DNA (CT-DNA) were purchased from Sigma-Aldrich, and plasmid DNA-pBR322 was obtained from TaKaRa Biotechnology. The cell cycle assay kit (Cycletest Plus DNA reagent kit) and apoptosis assay kit (Annexin V-FITC/PI apoptosis detection kit) were obtained from BD Biosciences. All buffer solutions were prepared with double distilled water, and further carried out of biological experiments.

The percentage composition of C, H and N of p-2-bmq were detected on a Flash EA 1112 elemental analyzer (Thermo Fisher Scientific, Waltham, MA, USA). FT-IR spectra of the complexes were detected on a PerkinElmer Fourier transform-IR spectrometer (Perkin Elmer, Waltham, MA, USA) in the region of 400–4000 cm^{-1} using KBr pellets. The MTT assay was measured on Tecan microplate reader (Tecan, Morrisville, NC, USA). DNA ladder was performed on G: BOX F3 gel imaging system (Syngene, UK). ICP-MS measurements were recorded by Nex ION 300× instrument (Perkin Elmer). Fluorescence staining method was observed on microscopic imaging systems of Carl Zeiss (Carl Zeiss, Jena, Germany) or Nikon (Nikon, Yokohama, Japan). All flow cytometry were detected by Guava easyCyte 6-2 L flow cytometer (Millipore, Billerica, MA, USA).

2.2. Synthesis

The pathway for the synthesis of 2-((1-(pyridin-2-yl)-1H-benzoimidazol-2-yl)methyl) quinolone (p-2-bmq) was prepared referring to the previous studies synthesis methods with some modifications (Scheme 1) [24,25].

2.2.1. Synthesis of Cu(p-2-bmq)Cl_2 (1)

The ligand of p-2-bmq (0.02 mmol, 0.0067 g) was dissolved in methanol (4 ml) and acetonitrile (2 ml) and then $CuCl_2$ (0.03 mmol, 0.0051 g) was added. The mixture system was stirred at room temperature to obtain a clear solution. The reaction vessel was placed at room temperature for several days, after evaporating to dryness, the block brown crystals were obtained. Yield: 73% (based on Cu). Anal. Calc. for $C_{22}H_{16}Cl_2CuN_4$ (%): C, 56.12; H, 3.43; N, 11.90. Found: C, 56.33; H, 3.45; N, 11.88. IR (KBr/pellet, cm^{-1}): 3574 (w), 3048 (w), 1592 (m), 1524 (w), 1474 (m), 1426 (m), 1382 (w), 1336 (m), 1152 (w), 1108 (w), 998 (w), 956 (w), 782 (w), 756 (s), 577 (w).

2.2.2. Synthesis of Zn(p-2-bmq)Cl_2 (2)

The synthetic process of complex **2** was referring to the method of complex **1** by adding $ZnCl_2$ (0.03 mmol, 0.0041 g), p-2-bmq (0.02 mmol, 0.0067 g), ethanol (4 ml), and dichloromethane (2 ml) to a reaction vessel. Finally, a yellow block crystal was obtained. Yield: 67% (based on Zn). Anal. Calc. for $C_{22}H_{16}Cl_2N_4Zn$ (%): C, 55.90; H, 3.41; N, 11.85. Found: C, 56.14; H, 3.27; N, 12.11. IR (KBr/pellet, cm^{-1}): 3494 (w), 3056 (w), 1593 (m), 1521 (w), 1474 (m), 1426 (m), 1385 (w), 1338 (m), 1151 (w), 1109 (w), 998 (w), 957 (w), 782 (w), 762 (s), 578 (w).

2.2.3. Synthesis of [co(p-2-bmq)Cl_2]$_2$ (3)

The synthetic method of complex **3** was same as the process of **1** by adding $CoCl_2$ (0.03 mmol, 0.0082 g), p-2-bmq (0.02 mmol, 0.0067 g), dichloromethane (2 ml), and ethanol (4 ml) to a reaction vessel. Finally, a brown block crystal was obtained. Yield: 72% (based on Co). Anal. Calc. for $C_{44}H_{32}Cl_4Co_2N_8$ (%): C, 56.67; H, 3.46; N, 12.02. Found: C, 57.78; H, 3.34; N, 11.67. IR (KBr/pellet, cm^{-1}): 3056 (w), 1648 (w), 1592 (s), 1520 (w), 1472 (m), 1422 (m), 1379 (w), 1337 (m), 1147 (w), 1105 (w), 995 (w), 951 (w), 823 (w), 756 (s), 578 (w).

2.3. X-ray crystallography

The single crystal X-ray diffraction data for complex **1** and **3** was collected on a Super Nova system with diffractometer equipped with mirror monochromatic Cu-Kα radiation (λ = 1.54184 Å) at 293(2) K. Crystallographic data for the complex **2** was equipped with mirror monochromatic Mo-Kα radiation (λ = 0.71073 Å) at 293(2) K. The structures were solved with direct methods and refined by full-matrix least-squares methods on F^2 using the OLEX2 and SHELXL [26,27]. The non-hydrogen atoms were located in anisotropic thermal parameters. The hydrogen atoms were added by theoretically. The crystallographic

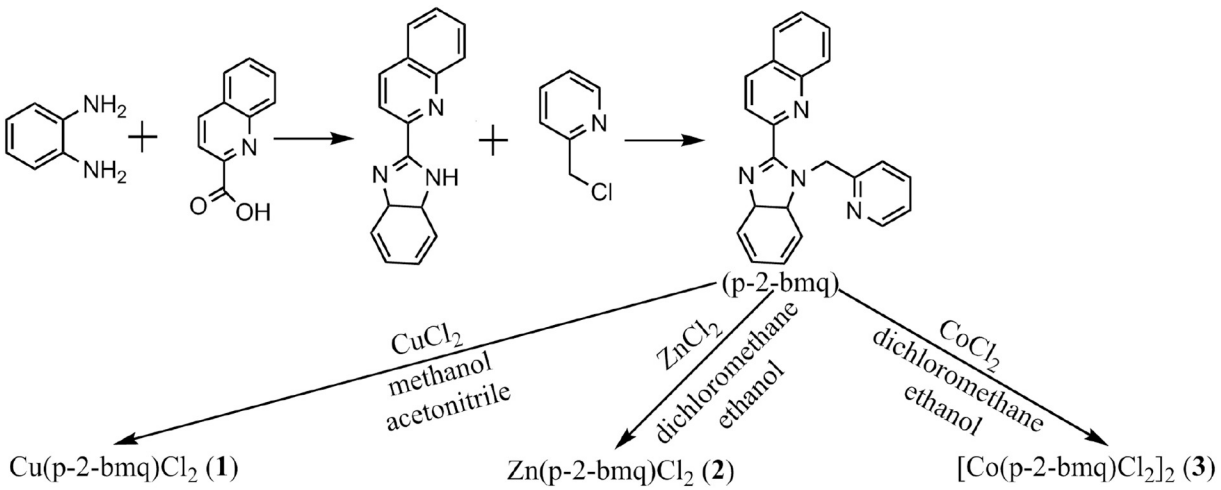

Scheme 1. The synthetic route of p-2-bmq and complexes **1–3**.

Table 1
Crystallographic data and structural refinement for complexes **1**, **2** and **3**.

	Complex **1**	Complex **2**	Complex **3**
Formula	$C_{22}H_{16}Cl_2CuN_4$	$C_{22}H_{16}Cl_2N_4Zn$	$C_{44}H_{32}Cl_4Co_2N_8$
Formula weight	470.834	472.66	932.44
Temperature/K	293(2)	293(2)	130(2)
λ (Cu, Mo Kα), Å	1.54184	0.71073	1.54184
Crystal system	triclinic	triclinic	triclinic
Space group	*P-1*	*P-1*	*P-1*
a (Å)	8.8218(5)	8.7155(5)	11.6818(7)
b (Å)	11.0113(7)	11.3466(6)	13.0638(5)
c (Å)	12.1126(7)	12.5573(6)	14.5928(8)
α(deg)	72.941(5)	67.873(5)	94.516(4)
β(deg)	88.599(5)	85.974(4)	104.816(5)
γ(deg)	81.618(5)	80.122(4)	113.085(5)
Volume ($Å^3$),*Z*	1112.62(11),2	1133.28(10),2	1940.03(17),2
Calculated density (g/cm^3)	1.405	1.334	1.596
F(000)	478.0	480.0	948.0
θ range for data (deg) collection (deg)	3.82 to 76.53	2.91 to 26.37	3.2 to 76.64
Limiting indices	$-10 \le h \le 10$ $-13 \le k \le 13$ $-15 \le l \le 13$	$-10 \le h \le 10$ $-14 \le k \le 12$ $-15 \le l \le 15$	$-14 \le h \le 14$ $-16 \le k \le 13$ $-18 \le l \le 18$
Reflections collected	9144	10,804	16,104
Independent reflections	4539 [*R*(int) = 0.0171]	4622 [R(int) = 0.0253]	7963 [R(int) = 0.0239]
Goodness-of-fit on F^2	1.064	1.066	1.028
Final *R* indexes [$I \ge 2\sigma$ (I)]	$R_1 = 0.03152$, $wR_2 = 0.0906$	$R_1 = 0.0385$, $wR_2 = 0.0994$	$R_1 = 0.0306$, $wR_2 = 0.0754$
R indexes [all data]	$R_1 = 0.0336$, $wR_2 = 0.0925$	$R_1 = 0.0529$, $wR_2 = 0.1075$	$R_1 = 0.0347$, $wR_2 = 0.0778$
Largest diff. Peak and hole (e $Å^{-3}$)	0.32/−0.56	0.41/−0.42	0.48/−0.43

data and single crystal structure parameters are listed in Table 1, and the parameters used for intensity collection are summarized in Table S1.

2.4. Cell culture

Four human esophageal cancer cell lines, including human colon carcinoma cell line (HCT116), human liver carcinoma cell line (SMMC7721), human gastric cancer cell line (BGC823), and human colorectal carcinoma cell line (HT29), were cultured in medium solution supplemented with FBS (10%), and 100 units/ml penicillin and 100 μg/ml streptomycin at 37 °C in humidified incubator with 5% CO_2. SMMC7721 and HT29 cells were grown and cultured in RPMI (Roswell Park Memorial Institute) cell culture medium solution, and HCT116 and BGC823 cells were seeded in DMEM (Dulbecco's modified Eagle's medium) cell culture medium solution.

2.5. Cytotoxicity assay

The cells were grown in 96-well plate (8×10^3 cells/well) for 24 h and allowed to adherence. After incubation with compounds for 24, 48 and 72 h, 20 μl MTT (5 mg/ml) solution was added to each well to further treatment for 4 h at 37 °C in the darkness. After incubation, the solution in each well was changed with 150 μl DMSO. The 96-well plates were shaken gently for 20 min on a plate shaker and the absorbance data (OD) was detected on a microplate reader at 492 nm. Cell survival rate was obtained from the percentage absorbance compared to that the control (untreated cells). The IC_{50} values were calculated according to the gradient concentrations of the compounds induced the 50% inhibition of cell growth. All tests were repeated in at least three times independently.

2.6. AO/EB and Hoechst 33258 staining analysis

The cells of SMMC7721 were seeded in 6-well plate and incubated with gradient concentrations of **1** (0, 15 and 30 μM) for 48 h. After treatment, the cell culture medium in the well was removed and washed three times with ice-cold PBS. Each well added cell immobilized solution (acetic acid: ethanol = 1:3, 1 ml) and then treated for 10 min at room temperature. The cells were counterstained with Hoechst 33258 (5 μg/ml) and AO/EB dual staining solution (100 μg/ml AO, 100 μg/ml EB) for 10 min in the darkness. The cells were imaged with Zeiss fluorescence microscope (Hoechst 33258 staining) and Nikon fluorescence microscope (AO/EB dual staining), respectively.

2.7. Single cell gel electrophoresis

The cells of SMMC7721 were seeded in 6-well plate and incubated with gradient concentrations of **1** (0, 15 and 30 μM) for 48 h. Then the culture medium was removed and the cells harvested by trypsinization. Preparing the first agarose layer with 0.5% low melting point agarose in PBS on slide, and continue to add 1% normal melting point agarose to deposit on the first layer to form the second layer. Actually, the second layer contained 10^4 cells. Furthermore, the layer with low melting point agarose was deposited on the second layer to protect the cell layer. After above manufacture, the samples were placed in lysis solution (2.5 M NaCl, 100 mM EDTA, 10 mM Tris, 1% Triton X − 100 and 10% DMSO, pH 10) at 4 °C for 3 h. After incubation, all samples were incubated with alkaline electrophoresis buffer (0.3 M NaOH, 1 mM EDTA, pH 13) for 20 min. Then the electrophoresis was carried out at 25 V for 20 min. After electrophoresis, the slides were transferred into neutralization buffer (0.4 M Tris, pH 7.5) and washed with it three times, and then the samples were stained with EB (5 mg/ml) in the darkness for 20 min. The samples were detected on Zeiss fluorescence microscopy.

2.8. Cellular uptake

The cells of SMMC7721 were incubated with complexes **1, 2** and **3** (10 μM) for 12 h. After treatment, 10^6 cells were collected separately. Besides, the intracellular components, including cytoplasm, mitochondria and nucleus, were separated with cell mitochondria isolation kit (Beyotime Institute of Biotechnology). All samples were mineralized by concentrated HNO_3 (100 μl) at 95 °C for 1 h. Then each tube was added 50 μl H_2O_2 (30%) to continue incubated at 95 °C for another 1 h. Add 100 μl concentrated HCl to each tube. The sample was continued incubation until it < 50 μl. Moreover, the cytoplasm was treated with ultrasonic crushing for 20 min. Finally, all samples were filtered

through a 0.22 μm millipore plastic membrane filter. The samples were observed on inductively coupled plasma mass spectrometry (ICP-MS) before diluted with Millipore water to 4 ml.

2.9. Intracellular reactive oxygen species (ROS) levels detection

The level of ROS intracellular was measured by the fluorescent dye 2′,7′-dichlorodihydro fluorescein diacetate (DCFH-DA) kit (Beyotime Institute of Biotechnology). SMMC7721 cells were incubated with medium containing different concentrations of **1** (0, 15 and 30 μM) for 24 h. After treatment, the cell culture medium was removed and the cells were harvested, and then the cells were stained by DCFH-DA dye at 37 °C in the darkness for 20 min. After incubation, the cells were centrifuged and washed with DMEM cell culture medium without FBS three times. All samples were detected on flow cytometry and further calculated by FlowJo software.

2.10. Mitochondrial membrane potential (ΔΨm) assay

SMMC7721 cells were treated with different concentrations of **1** (0, 15 and 30 μM) for 48 h. The cells were harvested and washed with ice-cold PBS, and then the cells were resuspended in JC-1 staining buffer (1 μg/ml) at 37 °C in the darkness for 20 min. After incubation, the cells were washed with DMEM cell culture medium without FBS three times to remove the unbound fluorescent dye. The data were obtained from flow cytometry and calculated by FlowJo software.

2.11. Annexin V-FITC/PI dual staining apoptosis analysis

After different concentrations of **1** (0, 15 and 30 μM) treatment for 48 h, SMMC7721 cells were harvested. The cells were washed with ice-cold PBS and resuspended in 1× binding buffer. Then the cells were incubated with the staining buffer at 37 °C for 30 min in the darkness. The fluorescent staining buffer contained Annexin V-FITC (50 μg/ml) and propidium iodide (1 mg/ml). The samples were ice-cold incubation in the darkness and 10,000 events were detected on flow cytometry with per sample.

2.12. Cell cycle arrest analysis

The SMMC7721 cells were incubated with the gradient concentrations of **1** (0, 15 and 30 μM) for 48 h. After treatment, the cells were obtained and performed according to the guide of BD Cycletest Plus DNA reagent kit. All samples were detected on flow cytometry, and 10,000 events were acquired per sample. Besides, the percentage of cells in different cell cycle phases was calculated by ModFit LT software.

3. Results and discussion

3.1. Description of the crystal structures

3.1.1. Crystal structure of Cu(p-2-bmq)Cl_2 (1)

Complex **1** is a mononuclear structure with one copper atom, one p-2-bmq ligand and tow chloride ions (as shown in Fig. 1a). The Cu(II) ion center shows a distorted square pyramidal geometry with four connected atoms, including two chloride ions (Cl1 and Cl2) and two nitrogen atoms from p-2-bmq ligand (N1 and N2). The distance between the metal center atom and the coordination N atom of quinoline (N1) is 2.0361(14) Å (Cu1–N1), and with the distance between metal ion and benzimidazole nitrogen atom is 1.9576(14) Å (Cu1–N2) [28,29]. Besides, the dihedral angle of two large conjugated systems containing benzimidazole ring and the quinoline ring is 4.6(3)°. Other selected bond distances and bond angles of **1** are listed in Table S1. As shown in Fig. S1, the π–π interaction between the adjacent to two molecules of pyridine (quinoline) and pyridine (quinoline) rings with 3.661(3) Å, imidazole and benzene (benzimidazolyl) rings with 3.504(3) Å, and pyridine (quinoline) and benzene (quinoline) rings from the adjacent to two molecules with 3.597(4) Å, respectively. Besides, the structure has a hydrogen bond of C17–H17···Cl1 with bond length of 3.663(6) Å (Table S2).

3.1.2. Crystal structure of Zn(p-2-bmq)Cl_2 (2)

As shown in Fig. 1b, the crystal structure of **2** is a mononuclear structure. The Zn(II) center is tetracoordinated and connected with two nitrogen atoms from p-2-bmq ligand and two chloride ion, showing a distorted tetrahedral geometry. The dihedral angle of benzimidazole and quinoline rings in two adjacent ligands is 7.72(17)°, which is bigger than the dihedral angle between the same conjugated rings in the complex **1**. This phenomenon may be caused by the Jahn-Teller distortion. The bond lengths and angles are listed in Table S1, and they are within the normal range reference from the previous studies [30]. As shown in Fig. S2, the 3D supramolecular structure of **2** is maintained by the π–π interactions. For the complex **2**, the π–π interaction between the adjacent to two molecules of pyridine (quinoline) and pyridine (quinoline) rings with 3.7100(17) Å, imidazole and benzene (benzimidazolyl) rings with 3.7102(18) Å, and pyridine (quinoline) and benzene (quinoline) rings from the adjacent to two molecules with 3.623(2) Å, respectively. In addition, no classic hydrogen bonds were found in complex **2**.

3.1.3. Crystal structure of [Co(p-2-bmq)Cl_2]$_2$ (3)

The structure of complex **3** is shown in Fig. 1c, which is a centrosymmetric binuclear structure. The molecular structure contains two Co(II) ions (Co1 and Co1a), two p-2-bmq ligands and four chloride anions. Each Co(II) center is pentacoordinate and showing a distorted square pyramidal geometry with surrounding by N1, N2, Cl1, Cl2 and Cl1a. The selected bond distances and bond angles are listed in Table S1, which are very well similar with the previously articles [31]. The 3D supramolecular structure of complex **3** is maintained by π–π stacking and intra- or intermolecular hydrogen bonding interactions (Fig. S3). The distance between imidazole and pyridine (quinoline) rings of centroid to centroid is 3.6157(12) Å, and with a dihedral angel of 3.39(10)°. The π–π interaction between the adjacent of two ligands of benzene (quinoline) and benzene (benzimidazolyl) rings with 3.5353(12), and the dihedral angel between of them is 2.4657°. The π–π stacking in complex **3**, including benzene (benzimidazolyl) and pyridine (quinoline) rings and pyridine and pyridine rings, is also plays an important role in maintaining its supramolecular structure. Besides, all the hydrogen bonds of complex **3** were listed in Table S2.

3.2. In vitro cytotoxicity studies

The cytotoxicity of **1**–**3** against four esophageal tumor cell lines, including SMMC7721, BGC823, HCT116 and HT29 was detected by the MTT assay [32]. The IC_{50} values of **1** are listed in Table 2, and the compounds **2**, **3**, p-2-bmp and cisplatin are shown in Table S3, S4, and S5, respectively. The complexes **1**–**3** inhibited the growth of the four esophageal tumor cells in time- and dose-dependent manners. The cytotoxicity assay shows that **1** exhibits the higher cytotoxicity than **2**, **3**, and p-2-bmq against four esophageal tumor cell lines under the same experimental condition. Especially, **1** is found to show the lowest IC_{50} value (15.89 ± 0.91 μM) toward SMMC7721 cells for 72 h. Additionally, the cell viability of **1** against four esophageal tumor cell lines is depicted in Fig. 2. We further performed antitumor mechanisms based on SMMC7721 cells treated with complex **1**. (See Table 3.)

3.3. Apoptosis assay by AO/EB and Hoechst 33258 staining

In cell apoptosis process, the cell may be occurred morphological changes, including cell shrinkage, chromatin condensation, karyopycnosis, nuclear fragmentation, and formation of apoptotic bodies

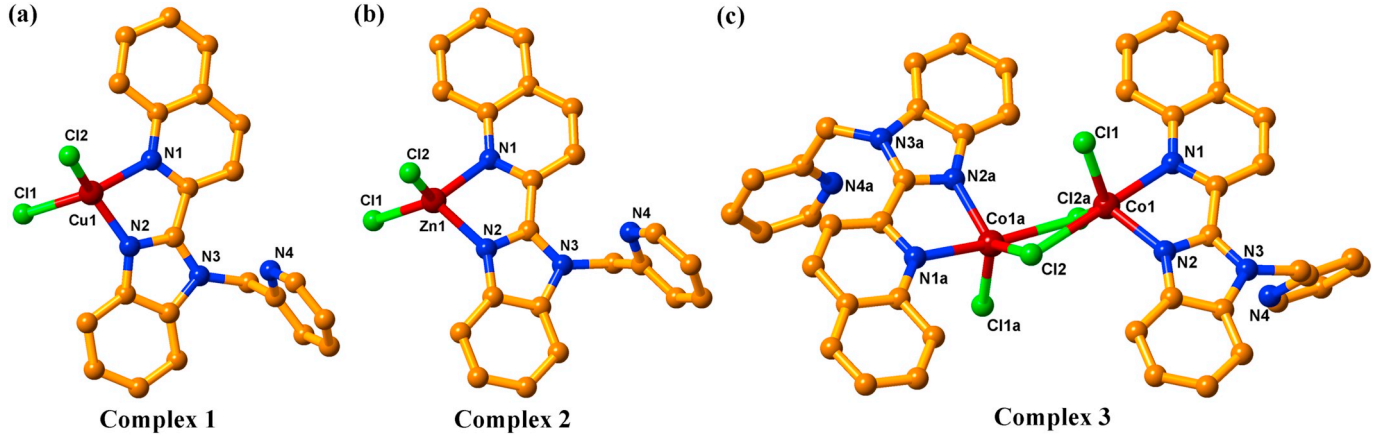

Fig. 1. The structures of Cu(p-2-bmq)Cl_2 (**1**), Zn(p-2-bmq)Cl_2 (**2**), and [Co(p-2-bmq)Cl_2]$_2$ (**3**), showing the atom labeling scheme.

[33]. The morphological changes of apoptosis induced by complex **1** were detected on fluorescence microscope with AO/EB and Hoechst 33258 staining. As shown in Fig. 3b and c, the cells were appeared apoptosis with gradient concentration of complex **1** treatment. Besides, the number of apoptotic cells showed to be dose-dependent manner. With Hoechst 33258 staining (Fig. 3d, e and f), the apoptotic cells were showed half-moon shaped nuclei, condensed chromatin and formed apoptotic bodies with bright blue fluorescence. The results indicated that complex **1** effectively induced SMMC7721 cells apoptosis.

3.4. Cellular uptake studies

The cellular uptake and localization of metal-based antitumor agents are important factors affecting cell physiological metabolism. The cellular uptake of metal-based complexes within SMMC7721 cells were measured by ICP-MS (Fig. 4, Table S6 and S7). The treatment of SMMC7721 cells with the complexes **1**–**3** led to a substantial increase in the cellular metal concentration compared to the untreated control. The results suggested that the metal content of cellular internalization were increased under the complexes incubation. As shown in Fig. 4a, the complex **1** was internalized by the cell about 27 times than control. However, the ratio of internalization of the complexes **2** and **3** by the cell was lower than that of the control. The results revealed that why the complex **1** more effective in cytotoxicity than the other two identical ligand-based complexes **2** and **3** under the same treatment. Moreover, the Cu content in the nucleus, mitochondria and cytoplasm was measured. As shown in Fig. 4b, the copper content in these three positions were increased, and the total intake of nucleus (70.13 ± 0.23 ng/10^6 cells) was higher than mitochondria (21.51 ± 0.44 ng/10^6 cells). It is possible that uptake of the complex **1** accumulated in nucleus or mitochondria in SMMC7721 cells, which might be induced apoptosis [34,35].

3.5. Intracellular ROS levels analysis

The expression level of ROS intracellular affects the aerobic metabolism of cells, even death and apoptotic cells can be overexpressed

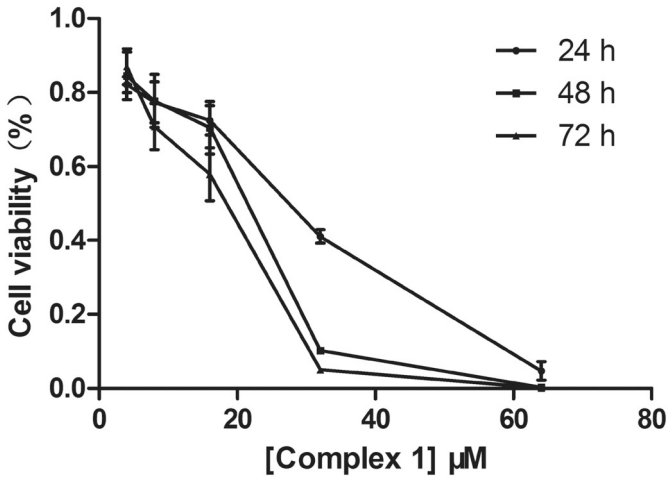

Fig. 2. Cell viability of SMMC7721 cells after treated with different concentrations of complex **1** for 24, 48 and 72 h, followed by MTT assay.

ROS [36]. The fluorescence probe of 2′,7′-dichlorodihydrofluorescein diacetate (DCFH-DA) is one of the most widely used techniques for directly measuring the redox state in cell, and it combines with intracellular esterases to become a non-fluorescent form (DCFH). Then DCFH can be used to convert fluorescent product (DCF) by means of intracellular free radicals. The fluorescence intensity of DFC reflects the level of expression of ROS intracellular [37,38]. As shown in Fig. 5, the green fluorescence intensity increased by the gradient concentration of **1** incubation. The leave of ROS intracellular was gradually increased, which was illustrated that internalization of complex **1** might be triggered the oxidative stress in SMMC7721 cells. [39] Moreover, ROS plays an important role in aerobic metabolism, ranging from apoptosis and necrosis to proliferation and carcinogenesis.

Table 2
The cytotoxicity of complex **1** against four human tumor cell lines for 24, 48 and 72 h.

Complex **1**	IC_{50} values (μM)[a]				
	SMMC7721	BGC823	HCT116	HT29	LO2
24 h	26.37 ± 0.32	41.83 ± 3.00	39.00 ± 3.15	45.55 ± 3.87	35.54 ± 1.23
48 h	18.81 ± 2.04	23.89 ± 3.42	29.92 ± 1.22	38.02 ± 2.74	29.37 ± 0.58
72 h	15.89 ± 0.91	21.66 ± 1.08	17.66 ± 1.03	20.41 ± 3.71	30.88 ± 1.70

[a] IC_{50} values are presented as the mean ± SD (standard error of the mean) from three independent experiments.

Table 3
The cytotoxicity of the ligand and cisplatin against four human tumor cell lines for 48 h.

Compounds	IC_{50} values (μM)[a]				
	SMMC7721	BGC823	HCT116	HT29	LO2
p-2-bmq	>100	>100	>100	>100	>100
Cisplatin	8.22 ± 0.77	8.00 ± 0.83	40.31 ± 0.69	47.69 ± 6.08	6.75 ± 0.21

[a] IC_{50} values are presented as the mean ± SD (standard error of the mean) from three independent experiments.

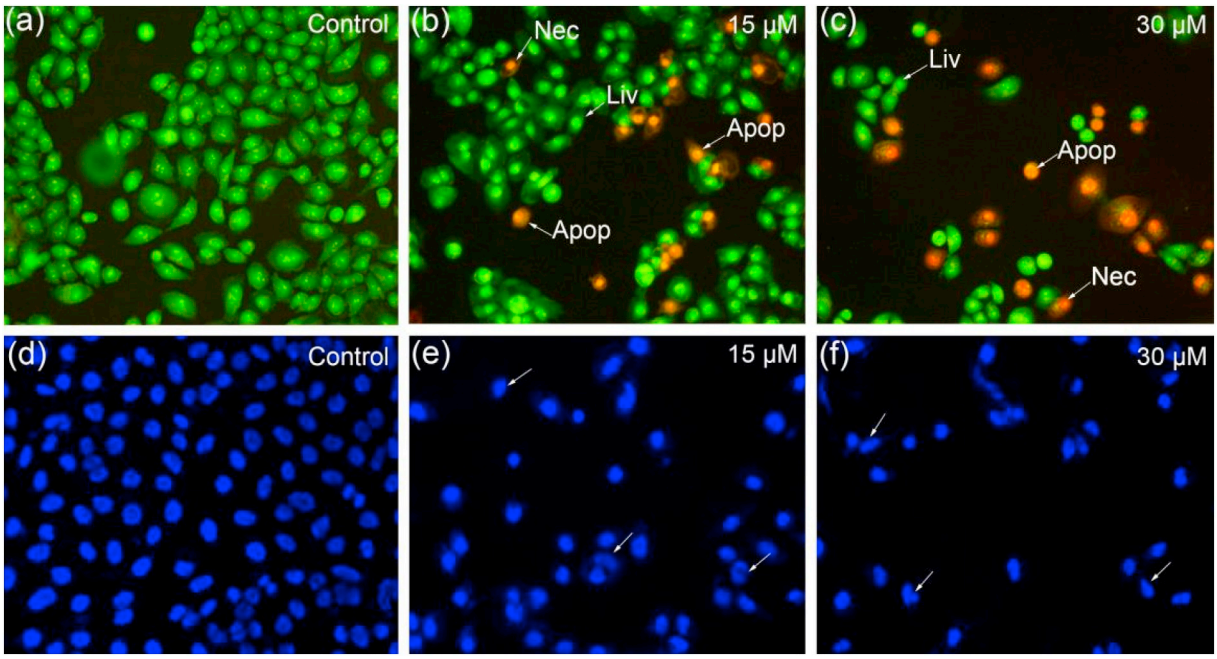

Fig. 3. Apoptosis assay by AO/EB (a, b, c with fluorescence microscope ×200 magnification) and Hoechst 33258 (d, e, f with fluorescence microscope ×400 magnification) staining methods of SMMC7721 cells upon treatment with **1** for 48 h. Nec, Liv and Apop: necrotic, living and apoptotic cells.

3.6. Single cell gel electrophoresis assay

The endogenous redox metabolism within the cells can alter intra- and inter-cellular communications and damage, especially inducing genomic nucleic damaged [39,40]. Comet assay was used to detect the DNA damage in SMMC7721 cells by incubation with **1**. As shown in Fig. 6a, the nuclei were showed round shape without incubation with **1**. However, the comet like tail appeared (Fig. 6b and c) after the cells were incubated with **1** at different concentrations for 48 h. These results indicate that complex **1** can cause DNA fragmentation and further induce apoptosis.

3.7. Detection of mitochondrial transmembrane potential (Δψm)

The loss of mitochondrial transmembrane potential causes mitochondrial dysfunction, further causing mitochondria to release apoptotic factors and activating apoptosis pathways leading to apoptosis [41]. Mitochondrial transmembrane potential (Δψm) was detected using the fluorescent probe of JC-1, which showed red fluorescence when it as aggregate form accumulates in the mitochondria of normal cells with high mitochondrial membrane potential. However, JC-1 was dispersed green fluorescence when it changes from aggregation to monomer with the Δψm lost [42]. As shown in Fig. 7, SMMC7721 cells

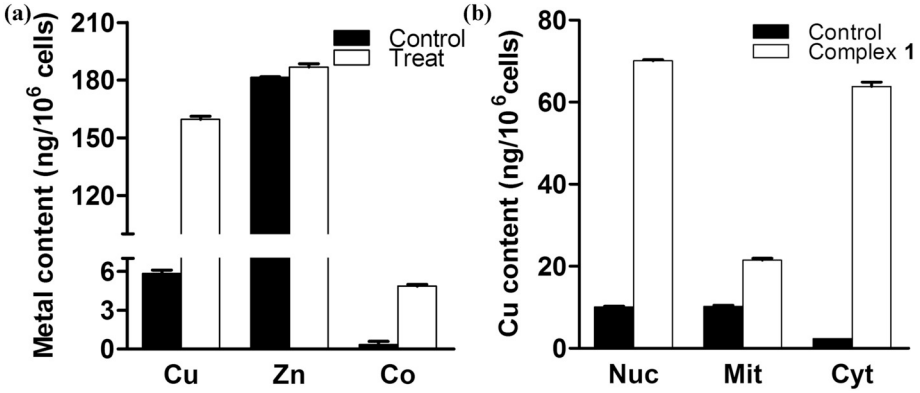

Fig. 4. SMMC7721 cells were treated with complexes **1**, **2** and **3**. Metal content in 10^6 cells (a) and copper content of nucleus, mitochondria and cytoplasm in 10^6 cells (b) were measured by ICP-MS. The mean ± SD (standard error of the mean) was obtained from three independent measurements for each test.

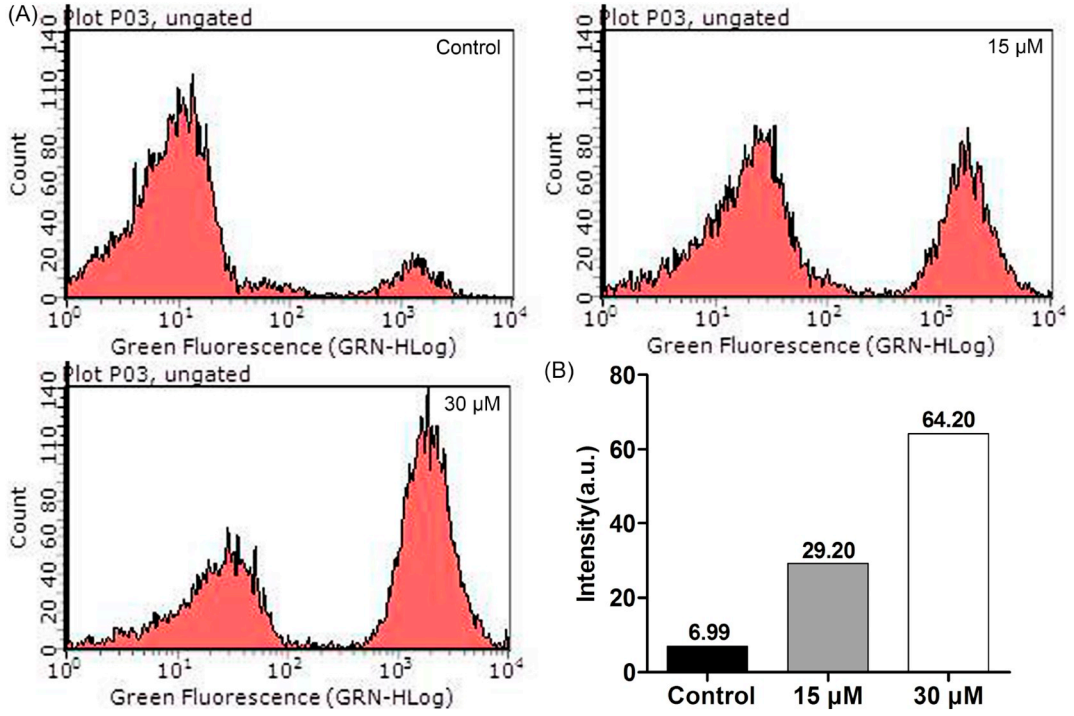

Fig. 5. The level of ROS intracellular was measured in SMMC7721 cells under incubation with **1**. (A) The data were obtained by flow cytometry. (B) The geometric mean intensity values of green fluorescence were detected by flow cytometry and calculated by FlowJo software.

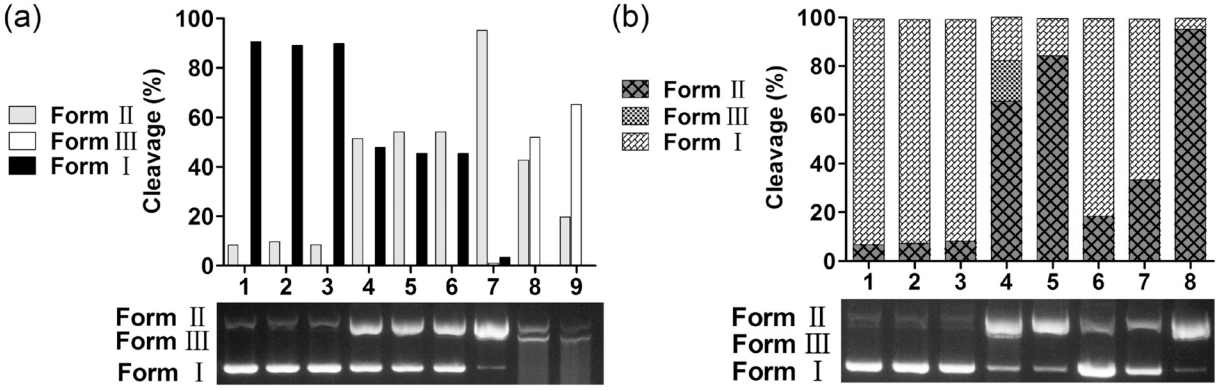

Fig. 6. a) Agarose gel electrophoresis patterns for the cleavage of pBR322 DNA by **1** at 37 °C after 4 h of incubation. Lane 1, DNA control; lane 2, DNA + Vc (1 mM); lane 3, DNA + **1** (120 μM); lane 4 to 9, DNA + Vc (1 mM) + **1** (20, 40, 60, 80, 100 and 120 μM, respectively). b) The DNA cleavage mechanisms of **1** were measured at 37 °C for 3 h incubation. Lane 1, DNA control; lane 2, DNA + Vc (1 mM); lane 3, DNA + **1** (120 μM); lane 4, DNA + Vc (1 mM) + SOD (30 units) + **1** (120 μM); lane 5, DNA + Vc (1 mM) + NaN_3 (1 mM) + **1** (120 μM); lane 6, DNA + Vc (1 mM) + EDTA (1 mM) + **1** (120 μM); lane 7, DNA + Vc (1 mM) + DMSO (1 mM) + **1** (120 μM); lane 8, DNA + Vc (1 mM) + **1**(120 μM).

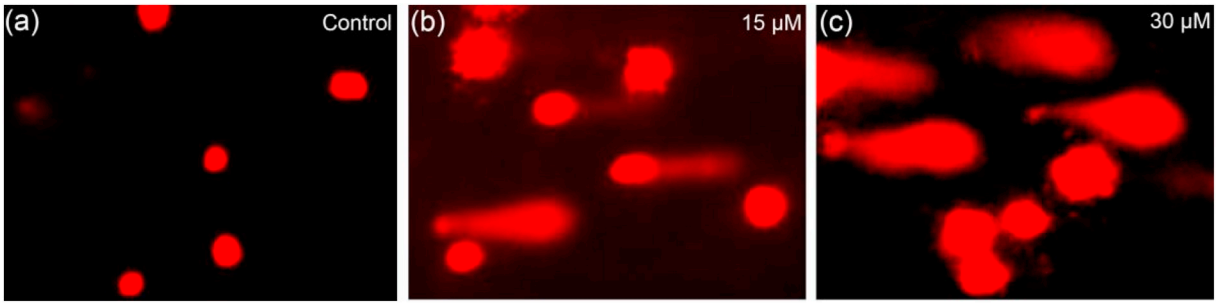

Fig. 7. SMMC7721 cells were incubation with **1** for 48 h. The single cell gel electrophoresis assay was measured by fluorescence microscopy with EB-stained (with fluorescence microscope ×400 magnification).

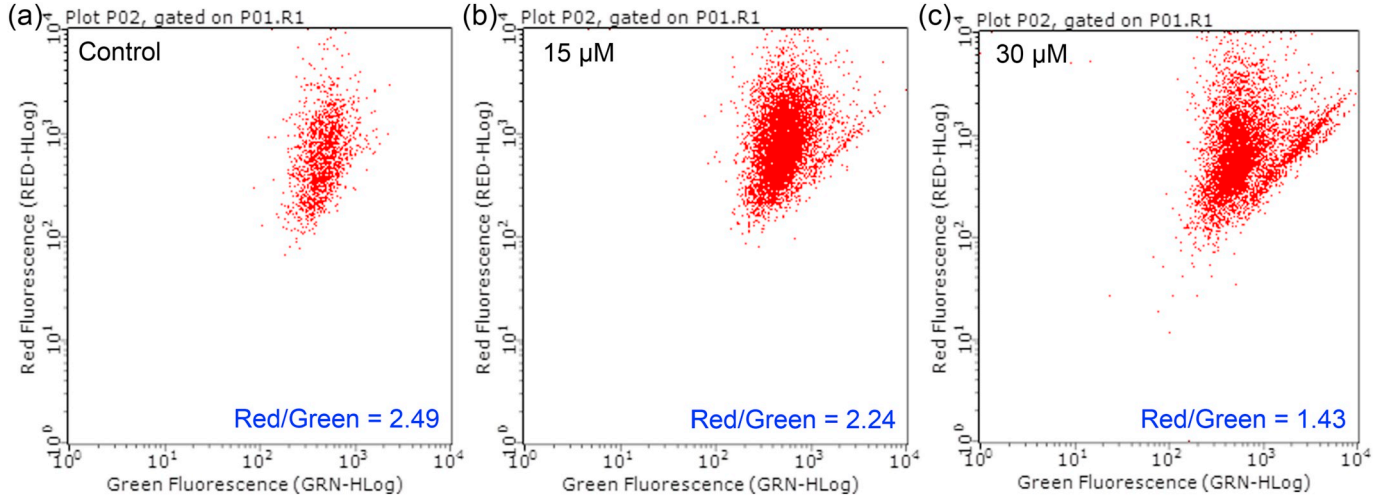

Fig. 8. Detection of SMMC7721 cell mitochondrial transmembrane potential with the fluorescence probe of JC-1 staining. The ratios of red/green fluorescent intensity were obtained from FlowJo software.

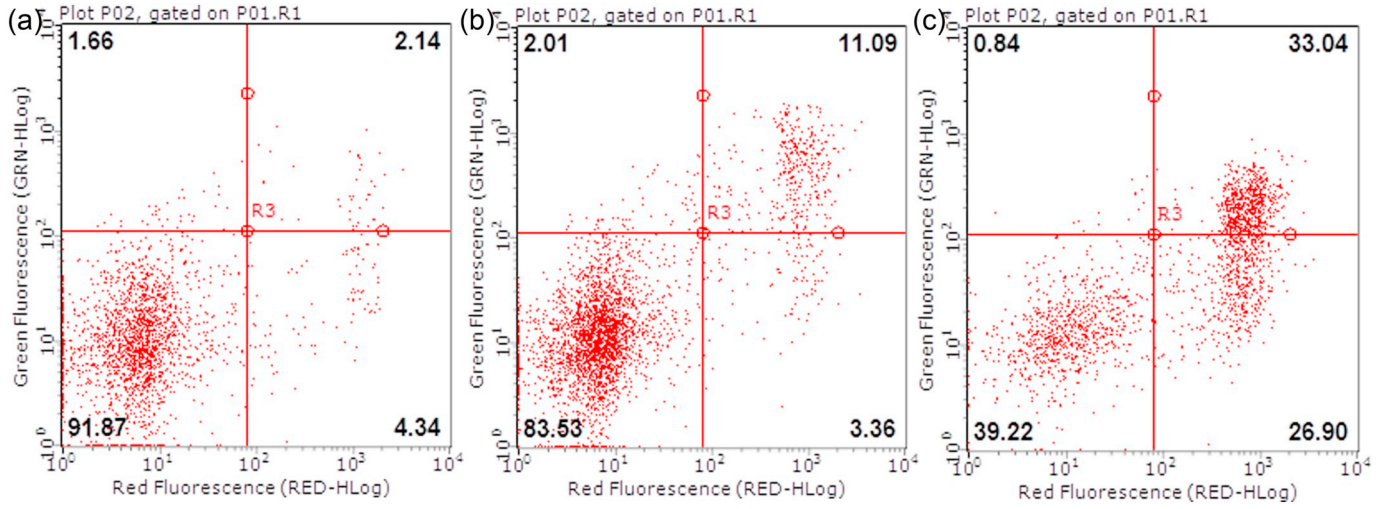

Fig. 9. SMMC7721 cells were treated with **1** (a, b and c for 0, 15 and 30 μM) for 48 h. The apoptosis data obtained from flow cytometry using the Annexin-VFITC/PI dual staining method.

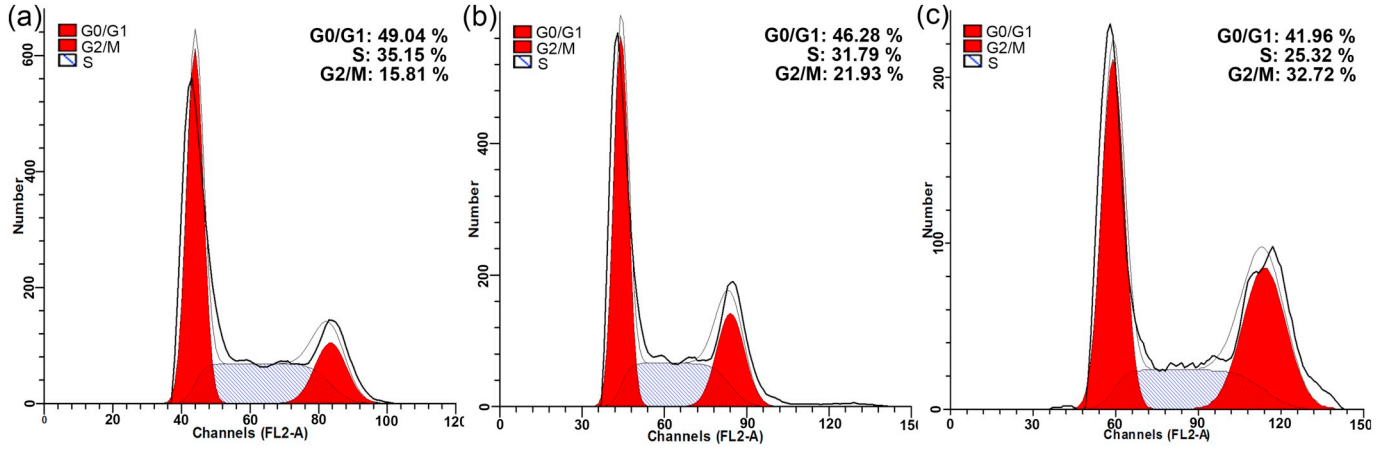

Fig. 10. SMMC7721 cells were treated with **1** (a, b and c for 0, 15 and 30 μM) for 48 h. Cell cycle phase data obtained from flow cytometry and analyzed by ModFit LT software.

were treated with gradient concentrations **1** for 48 h. The ratio of red/green fluorescence intensity has changed from 2.49 to 1.43, which was indicated that the red fluorescence intensity decreases and the green fluorescence intensity increases. These results suggest that the mitochondria transmembrane potential appeared depolarization.

3.8. Annexin V-FITC/PI dual staining apoptosis analysis

Phosphatidylserine (PS) is an asymmetrically phospholipid in normal cells , which is always distributed in the inner layer of the plasmamembrane. When cells develop early apoptosis, PS will be turned from the inner layer of the plasmamembrane to the outer layer [43]. The fluorescence probe of Annexin V is often used to quantify the externalization PS, which can be sensitively bond to PS by a Ca^{2+} dependent manner [44]. In the necrotic cells, PS externalization was also appeared, there would be used the fluorescence probe of PI to enable to detect the membrane disruption cells, and further to distinguish from apoptotic cells. The cells were dual staining with Annexin V-FITC (for the early apoptotic cells) and PI (for the late necrotic or necrotic cells). As shown in Fig. 8, the cells were incubated with Annexin V-FITC/PI, the percentage of the apoptotic cells (including early and late apoptotic cells) was changed from 6.48% to 59.94%. The result suggested that complex **1** can induce SMMC7721 cells apoptosis and with a dose-dependent manner in the apoptotic cell population.

3.9. Cell cycle arrest analysis

The *in vitro* quantification of the cellular DNA content in cell by flow cytometry aim to identify the cell cycle distribution and further to explore the anticancer mechanism. The relative cellular DNA content and distribution of SMMC7721 cells were shown in Fig. 9, the percentage of SMMC7721 cells in G0/G1 phase in control is 49.04%, and then it became 46.28% and 41.96% after incubation with 15 and 30 μM of complex **1**. Meanwhile S phase was decreased from 35.15% in control to 31.79% and 25.32% in treat groups. However, the percentage of G2/M phase was increased significantly, ranging from 15.81% in control to 21.93% and 32.72% upon the treatment with **1**. It suggested that **1** effectively blocked the cell cycle progression by G2/M phase arrest and exhibited a dose-dependent manner of antiproliferative mechanism. (See Fig. 10.)

4. Conclusions

In this paper, three new benzo-N-heterocycles derivatives were synthesized and characterized with 2-((1-(pyridin-2-yl)-1H-benzoimidazol-2-yl)methyl) quinolone ligand. The complexes were screened for cytotoxicity against four different esophageal cancer cell lines, which were exhibited different degrees inhibiting cell proliferation in time- and dose-dependent manners. Especially, complex **1** showed the highest cytotoxicity with IC_{50} value (15.89 ± 0.91 μM) toward SMMC7721 cells for 72 h. Moreover, complex **1** induced apoptosis by resulting in intracellular ROS increase, mitochondrial potential collapse, nucleus damaged and cell cycle arrest. Mechanistic studies of apoptosis induced by complex **1** reveal that endogenous metal-based complex induced intracellular metabolism imbalance, causing mitochondrial dysfunction and cellular DNA damage. These results may be promising development of benzo-N-heterocycles transition metal complexes used as potential chemotherapy agents. More detailed mechanisms of antitumor are currently being explored.

Acknowledgments

We gratefully acknowledge the financial support by National Natural Science Foundation of China Grant (No. 81402309), Training Scheme for Young Key Teachers of Colleges and Universities of Henan (No. 2016GGJS-139), Scientific Research Promotion Project of Henan University of Urban Construction (Nos. 2016QY017), and the Funding Program for Academic Technology Leaders of Henan University of Urban Construction (No. YCJXSJSDTR201705).

Appendix A. Supplementary data

Data Center, CCDC <1,897,549, 1,897,548 and 1,897,547> contains the supplementary crystallographic data for **1**, **2** and **3**. These data can be obtained free of charge *via* www.ccdc.cam.ac.uk/conts/retrieving.html, or from the Cambridge Crystallographic Data Centre, 12 Union Road, Cambridge CB2 1EZ, UK; fax: +441,223–336-033 or e-mail: deposit@ccdc.cam.ac.uk. Supplementary data to this article can be found online at doi: https://doi.org/10.1016/j.jinorgbio.2019.110816.

References

[1] P.C. Bruijnincx, P.J. Sadler, Curr. Opin. Chem. Biol. 12 (2008) 197–206.
[2] T.C. Johnstone, K. Suntharalingam, S.J. Lippard, Chem. Rev. 116 (2016) 3436–3486.
[3] W. Xiaoyong, G. Zijian, Chem. Soc. Rev. 42 (2012) 202–224.
[4] N. Muhammad, Z. Guo, Curr. Opin. Chem. Biol. 19 (2014) 144–153.
[5] P.C.A. Bruijnincx, P.J. Sadler, Curr. Opin. Chem. Biol. 12 (2008) 197–206.
[6] G. Nora, S.J. Lippard, Adv. Drug Deliv. Rev. 64 (2012) 993–1004.
[7] P. Zhang, P.J. Sadler, Eur. J. Inorg. Chem. 2017 (2017) 1541–1548.
[8] Z.H. Chohan, S.H. Sumrra, M.H. Youssoufi, T.B. Hadda, Eur. J. Med. Chem. 45 (2010) 2739–2747.
[9] G. Gasser, N. Metzler-Nolte, Curr. Opin. Chem. Biol. 16 (2012) 84–91.
[10] B. Bertrand, P.E. Doulain, C. Goze, E. Bodio, Dalton Trans. 45 (2016) 13005–13011.
[11] K. Sachiko, C. Horacio, K. Michiaki, K. Akihiro, T. Yasuko, S. Masaki, A. Ichio, N. Nobuhiro, T. Toru, K. Kazunori, Cancer Res. 70 (2010) 7031–7041.
[12] D. C, W. AR, Metallomics 4 (2012) 127.
[13] P. Daniela, C. Alessandra, S.M. Bárbara, P. Sante, G. Mauro, M. Sabrina, D.B. Loredana, Dalton Trans. 42 (2013) 9679–9687.
[14] M.C. Heffern, Y. Natsuho, R.J. Holbrook, A.L. Eckermann, T.J. Meade, Curr. Opin. Chem. Biol. 17 (2013) 189–196.
[15] Y. Samuni, S. Goldstein, O.M. Dean, M. Berk, BBA - General Subjects 1830 (2013) 4117–4129.
[16] G. Gasser, I. Ott, N. Metzler-Nolte, J. Med. Chem. 54 (2011) 3.
[17] M. Schenone, V. Dančík, B.K. Wagner, P.A. Clemons, Nat. Chem. Biol. 9 (2013) 232–240.
[18] A. Kamal, G.B. Kumar, V.L. Nayak, V.S. Reddy, A.B. Shaik, M.K. Reddy Rajender, Med.chem.commun. 6 (2015) 606–612.
[19] B. Narasimhan, D. Sharma, P. Kumar, Med. Chem. Res. 21 (2012) 269–283.
[20] K. Shah, S. Chhabra, S.K. Shrivastava, P. Mishra, Med. Chem. Res. 22 (2013) 5077–5104.
[21] B. Yogita, S. Om, Bioorg. Med. Chem. 20 (2012) 6208–6236.
[22] X.B. Fu, J.J. Zhang, D.D. Liu, Q. Gan, H.W. Gao, Z.W. Mao, X.Y. Le, J. Inorg. Biochem. 143 (2015) 77–87.
[23] L. Shenggui, C. Wenqiang, Y. Lianling, Z. Wenjie, L. Linlin, F. Cundong, C. Tianfeng, Dalton Trans. 42 (2013) 5932–5940.
[24] A.W. Addison, P.J. Burke, J Heterocycl Chem 18 (1981) 803–805.
[25] N. Martin, J.-C.G. Bünzli, V. McKee, C. Piguet, G. Hopfgartner, Inorg. Chem. 37 (1998) 577–589.
[26] O.V. Dolomanov, L.J. Bourhis, R.J. Gildea, J.A. Howard, H. Puschmann, J. Appl. Crystallogr. 42 (2009) 339–341.
[27] G.M. Sheldrick, Acta Crystallogr. Sect. C-Struct. Chem. 71 (2015) 3–8.
[28] X. Qiao, Z.-Y. Ma, J. Shao, W.-G. Bao, J.-Y. Xu, Z.-Y. Qiang, J.-S. Lou, Biometals 27 (2014) 155–172.
[29] N. Donappa, S. Naikar, Asian J. Chem. 5 (1993) 995.
[30] M. Wałęsa-Chorab, R. Banasz, D. Marcinkowski, M. Kubicki, V. Patroniak, RSC Adv. 7 (2017) 50858–50867.
[31] R. Kapoor, A. Kataria, P. Kapoor, P. Venugopalan, Transit. Met. Chem. 29 (2004) 425–429.
[32] T. Mosmann, J. Immunol. Methods 65 (1983) 55–63.
[33] H.R. Zhang, Y.C. Liu, T. Meng, Q.P. Qin, S.F. Tang, Z.F. Chen, B.Q. Zou, Y.N. Liu, H. Liang, Med.chem.commun. 6 (2015) 2224–2231.
[34] E.A. Prokhorova, A.V. Zamaraev, G.S. Kopeina, B. Zhivotovsky, I.N. Lavrik, Cellular & Molecular Life Sciences Cmls 72 (2015) 4593–4612.
[35] G. Kroemer, J.C. Reed, Nat. Med. 1 (2001) 513–519.
[36] M.L. Circu, T.Y. Aw, Free Radic. Biol. Med. 48 (2010) 749–762.
[37] C. Xiuping, Z. Zhangfeng, X. Zengtao, C. Lidian, W. Yitao, Free Radic. Res. 44 (2010) 587–604.
[38] J.S. Armstrong, K.K. Steinauer, B. Hornung, J.M. Irish, P. Lecane, G.W. Birrell, D.M. Peehl, S.J. Knox, Cell Death Differ. 9 (2002) 252.
[39] J.M. Matés, J.A. Segura, F.J. Alonso, J. Márquez, Arch. Toxicol. 82 (2008) 273–299.
[40] S.P. Jackson, B. Jiri, Nature 461 (2009) 1071–1078.
[41] D.R. Green, J.C. Reed, science 281 (1998) 1309–1312.
[42] M. Reers, T.W. Smith, L.B. Chen, Biochem 30 (1991) 4480–4486.
[43] V.A. Fadok, D.L. Bratton, S.C. Frasch, M.L. Warner, P.M. Henson, Cell Death Differ. 5 (1998) 551–562.
[44] I. Vermes, C. Haanen, H. Steffens-Nakken, C. Reutelingsperger, J.immunol.methods 184 (1995) 39–51.